RESEARCH ARTICLE

Inferring time of infection from field data using dynamic models of antibody decay

Benny Borremans[1,2,3] | Riley O. Mummah[1] | Angela H. Guglielmino[1] |
Renee L. Galloway[4] | Niel Hens[2,5] | K. C. Prager[1] | James O. Lloyd-Smith[1]

[1]Ecology and Evolutionary Biology Department, University of California Los Angeles, Los Angeles, California, USA

[2]I-BioStat, Data Science Institute, Hasselt University, Hasselt, Belgium

[3]Evolutionary Ecology Group, University of Antwerp, Antwerpen, Belgium

[4]Centers for Disease Control and Prevention, Atlanta, Georgia, USA

[5]Centre for Health Economic Research and Modelling Infectious Diseases, Vaccine & Infectious Disease Institute, University of Antwerp, Antwerpen, Belgium

Correspondence
James O. Lloyd-Smith
Email: jlloydsmith@ucla.edu

Funding information
Cooperative Ecosystem Studies Unit Cooperative Agreement, Grant/Award Number: W9132T1920006; Defense Advanced Research Projects Agency, Grant/Award Number: D18AC00031; H2020 Marie Skłodowska-Curie Actions, Grant/Award Number: 707840; National Science Foundation, Grant/Award Number: DEB-1557022, DEB-2245631 and OCE-1335657; Strategic Environmental Research and Development Program, Grant/Award Number: RC-2635; UCLA AIDS Institute and Charity Treks

Handling Editor: Matthew Silk

Abstract

1. Studies of infectious disease ecology would benefit greatly from knowing when individuals were infected, but estimating this time of infection can be challenging, especially in wildlife. Time of infection can be estimated from various types of data, with antibody-level data being one of the most promising sources of information. The use of antibody levels to back-calculate infection time requires the development of a host-pathogen system-specific model of antibody dynamics, and a leading challenge in such quantitative serology approaches is how to model antibody dynamics in the absence of experimental infection data.

2. We present a way to model antibody dynamics in a Bayesian framework that facilitates the incorporation of all available information about potential infection times and apply the model to estimate infection times of Channel Island foxes infected with *Leptospira interrogans*.

3. Using simulated data, we show that the approach works well across a broad range of parameter settings and can lead to major improvements in infection time estimates that depend on system characteristics such as antibody decay rate and variation in peak antibody levels after exposure. When applied to field data we saw reductions up to 83% in the window of possible infection times.

4. The method substantially simplifies the challenge of modelling antibody dynamics in the absence of individuals with known infection times, opens up new opportunities in wildlife disease ecology and can even be applied to cross-sectional data once the model is trained.

KEYWORDS
antibody decay, bayesian dynamic model, disease ecology, incidence, quantitative serology, time of infection, transmission dynamics, wildlife disease

1 | INTRODUCTION

Knowing when individuals got infected with a pathogen can dramatically boost insights into infectious disease biology, at both population and within-host scales (Handel & Rohani, 2015; Pepin et al., 2017). This knowledge allows estimation of incidence and force of infection, fundamental quantities for understanding and modelling transmission dynamics (Heisey et al., 2006; Held et al., 2019; Hens et al., 2010) and developing mitigation strategies (Caley & Hone, 2004; Weitz et al., 2020).

Individual infection times are relevant to a broad range of pathogen-related factors, including interpreting timelines of clinical disease (Hawley et al., 2011), vaccine efficacy (Antia et al., 2018), infection risk factors (Borremans et al., 2011; Pepin et al., 2019), pathogen spillover (Smith et al., 2014), effects of disease on wildlife health and survival (Tersago et al., 2012), host immunity (Epstein et al., 2013) and tracing infection sources (Craft, 2015). However, even though a variety of data can theoretically be used to estimate infection time (e.g. clinical disease signs, antibody concentration, outbreak seasonality, contact tracing), there are significant challenges that limit the widespread adoption of time-of-infection approaches, particularly in wildlife.

Key challenges include incorporating individual variation in response to infection (Simonsen et al., 2009; Teunis et al., 2002), integrating different data sources (Borremans et al., 2016), dealing with interval-censored data (Wilber et al., 2020), modelling the anamnestic response to reinfection (Pothin et al., 2016) and dealing with antibody cross-reactivity. A currently unresolved major challenge is how to model the dynamics of biomarkers such as antibodies or pathogen DNA/RNA when there are no individuals with a known infection time, such as a group of animals infected experimentally and tracked longitudinally; this challenge is particularly common in wildlife studies.

Models of biomarker dynamics constitute the foundation of most time-of-infection estimation methods (Brookmeyer & Gail, 1988; Gilbert et al., 2013; Teunis et al., 2016) and are central to the rapidly expanding field of quantitative serology (Boni et al., 2019; Hay et al., 2020; Pepin et al., 2017; Teunis et al., 2012). The presence and concentration of biomarkers can contain information about whether and when an individual has been infected (Borremans et al., 2016), the degree of immunity (Röltgen et al., 2021), infection severity (Vaughn et al., 2000), and whether and for how long they are infectious (Hardestam et al., 2008; Prager et al., 2020). Crucially, a biomarker can be used for such purposes only after its relevant properties have been quantified and when a model exists of how its presence or concentration correlates with the information of interest (e.g. time since infection).

Antibody dynamics can be a particularly rich source of information about the time of infection. Following infection, antibody levels decline after reaching a peak level sometime after infection, and this decay tends to follow a particular functional form, with a characteristic decay rate, specific to a host-pathogen system and antibody type. When this functional form and rate are known, antibody levels measured at some later point can potentially be used to determine how long ago an individual was infected (Boni et al., 2019; Hay et al., 2020; Teunis et al., 2012). This, in turn, opens up the possibility to improve estimates of incidence in the population (Hay et al., 2020; Pepin et al., 2017; Wilber et al., 2020) and perhaps to estimate whether and for how much longer an individual is immune to reinfection (Borremans et al., 2015). Notably, R package ꜱᴇʀᴏꜱᴏʟᴠᴇʀ (Hay et al., 2020) provides a range of functions to infer infection histories based on antibody dynamics and offers a framework that is able to account for cross-reactivity and antibody boosting following re-exposure. The models in this package are powerful, but their usefulness depends on how well the underlying antibody dynamic model can be estimated.

Antibody dynamic models typically follow a general pattern: an increasing phase (often ignored because it is short), a peak level and a decay phase (Teunis et al., 2016). Quantifying this pattern and its associated parameters requires specific data. The optimal situation for parameter estimation is to have experimental data with known infection times for multiple individuals that are sampled longitudinally until antibodies are no longer detectable. For example, experimental infection of the African rodent *Mastomys natalensis* with an arenavirus, followed by frequent sampling for the entire lifetime, enabled the development of an antibody dynamic model that could then be used to estimate infection times of wild rodents based on a limited number of samples (Borremans et al., 2015, 2016). Similarly, experimental data on influenza A in snow geese and mallards have been used to model the antibody response following infection and subsequently estimate infection times and force of infection (Pepin et al., 2017).

Unfortunately, in most wildlife disease studies such experimental data are not feasible to collect, and infection times in the field are unknown. This is particularly problematic when periods between sampling are long and sample sizes are small (Gilbert et al., 2013). This has been a major reason that quantitative serology methods have not yet been widely adopted in wildlife disease ecology (Gilbert et al., 2013). Instead, a standard approach to determining infection time has been to take the midpoint between the interval bounded by the last antibody-negative and the first positive samples (Begon et al., 2009; van den Bergh et al., 2019) or to consider this interval as a uniform probability distribution for infection (i.e. any time is equally possible). Intervals of multiple months or even years are common in wildlife systems, leading to potentially large errors surrounding the time of infection estimates, especially when a uniform distribution between sampling times is assumed. This offers opportunities for improvement, as quantitative serology models that improve on these interval-censored uniform distributions have the potential to provide better estimates of infection time, which could dramatically improve related estimates of epidemiological quantities such as incidence.

Here, we present a general approach for modelling antibody dynamics when sampling is sparse and infection times are unknown (Figure 1). The approach uses hierarchical Bayesian MCMC inference to integrate different sources of information about model
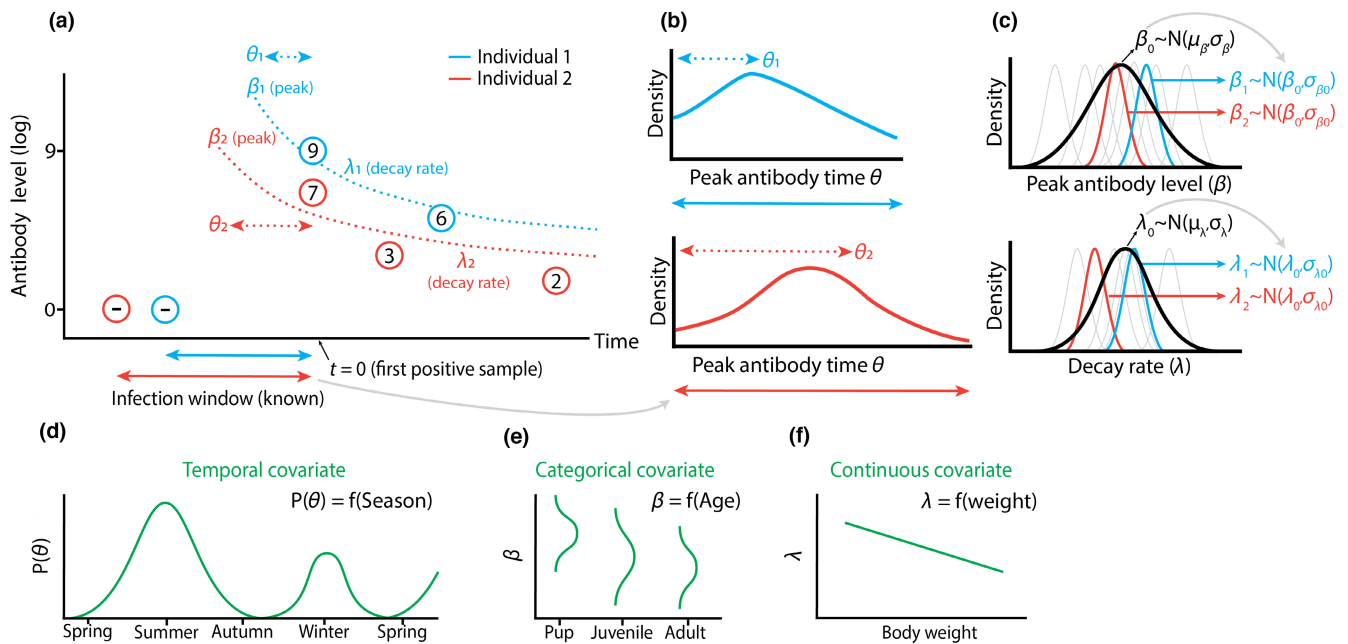
FIGURE 1 Hierarchical Bayesian modelling of biomarker data to estimate infection times. Bayesian inference offers a framework to use multiple sources of information to construct biomarker models and estimate individual time of infection. Panel (a) illustrates observed $\log_2$ antibody level data (circled numbers) for two individuals that are used to estimate model parameters β (peak antibody level) and λ (decay rate), with the ultimate goal of estimating the time of infection for each individual i (which is determined by the peak antibody time θ_i, measured relative to the time of the first positive sample) Dotted lines show possible unobserved antibody trajectories. Intervals between the last negative and first positive samples can be used as prior information to bound possible peak antibody times θ_i (Panel b: posterior probabilities indicating the most likely peak antibody times). Model parameters can be estimated at the individual level (β_i and λ_i), while simultaneously estimating the mean and variation of these parameters at the population level (β_0, $\sigma_{\beta0}$, λ_0, $\sigma_{\lambda0}$) in a hierarchical way (c). When available (not in our study), other types of information can be used to improve estimates of the different model parameters, for example, seasonal fluctuations in infection risk provide information about θ_i (d), while age-dependent infection risk (e) or a continuous covariate such as body weight (f) can provide information about β_i or λ_i.

parameters, with full consideration and propagation of uncertainty, and accounting for population heterogeneity in antibody decay characteristics. Additionally, we show how the simultaneous integration of the dynamics of additional biomarkers can improve parameter fitting and infection time estimation. We apply this approach to island foxes *Urocyon littoralis* infected with *Leptospira interrogans* serovar Pomona, using standard non-experimental field data only. The framework provides a way to estimate infection times by modelling biomarker dynamics even in the absence of experimental data, which we hope will stimulate more widespread use of quantitative serology in disease ecology.

2 | MATERIALS AND METHODS

2.1 | Data collection

Serum samples from island foxes were collected on Santa Rosa Island (California, USA) as part of a reintroduction and monitoring program (Coonan et al., 2015). Sampling was done annually between July and February, from 2004 through 2019. Foxes were trapped using Tomahawk Live Traps (Tomahawk, WI, USA). Passive integrated transponder (PIT) tags were used for identification. Foxes

were weighed, aged and assessed for body condition. Samples were collected during capture, taking up to 10 mL of blood. Blood was kept cold until centrifuging 3–5 h later, after which serum samples were frozen. Samples were tested for antibodies against *Leptospira* using microscopic agglutination testing (MAT). Samples prior to 2016 were tested at the Centers for Disease Control (CDC; Atlanta, Georgia, USA), and later, the samples were tested at the Animal Health Diagnostic Center (Ithaca, New York, USA). The samples were titrated to endpoint titre against serovar Pomona. Samples tested at CDC before 2013 were also titrated to endpoint titre for serovar Autumnalis. Antibody levels were log-transformed so that each unit change corresponds with a two-fold dilution step ($\log_2\left(\frac{dilution}{100}\right) + 1$). All trapping and sampling were done by the National Park Service under USFWS permit TE-08267-2. More details can be found in (Coonan, 2010).

We used antibody levels against *Leptospira interrogans* serovars Pomona and Autumnalis for antibody decay modelling and peak antibody time estimation. While the study population is known to be infected with serovar Pomona (Mummah, 2021), antibodies show a strong MAT signal for both serovar Pomona and serovar Autumnalis due to cross-reactivity (Levett, 2003). We leveraged both data sources to improve model parameter fitting and infection time estimation.

2.2 | Candidate models

Prior to model fitting, candidate models of antibody decay had to be chosen. Aspects to keep in mind when selecting candidate models are the possible shapes a function can have and the number of unknown function parameters. A model with more parameters has increased flexibility, but this can increase the risk of overfitting and reduce the model's ability to predict new data (Bolker, 2008). Several functions have been used to model antibody decay, with the single (constant decay rate) and double (gradually decreasing decay rate) exponential functions being the most common (Boni et al., 2019; Teunis et al., 2016). When initial decay is significantly faster than later decay, alternatives such as a power function can be used (Teunis et al., 2016). When empirical antibody kinetics do not resemble existing functions, a flexible function such as a smoothed spline can be used (Borremans et al., 2016). Note that it is useful to consider and compare multiple models, as this will reduce the chances of relying on a misspecified model that results in false confidence in parameter estimates. Even though Bayesian models offer the advantage of providing a full posterior distribution that allows proper quantification of estimation uncertainty, it is nevertheless important to choose the underlying models wisely.

Based on initial data exploration we selected three candidate functions. Single exponential: $\mu_{i,t} = \beta_i e^{-\lambda_i(t+\theta_i)}$; double exponential: $\log(\mu_{i,t}) = \log(\beta_i)e^{-\lambda_i(t+\theta_i)}$; power: $\log(\mu_{i,t}) = \frac{1}{1-r_i}\log\left(\beta_i^{(1-r_i)} - (1-r_i)v_i(t+\theta_i)\right)$; where $\mu_{i,t}$ is the observed antibody level of individual i sampled at time t. Here, t is defined as the time since an individual's first positive sample and θ_i is the time of peak antibody level relative to the first observed positive sample of individual i (i.e. the number of days between an individual's estimated time of peak antibody level and its first observed positive sample). β_i and λ_i are the peak antibody level and antibody decay rate of individual i. r_i and v_i are the shape and scale parameters of the power function. Functions were fitted separately to Pomona and Autumnalis, not considering mixed functions (e.g. a single exponential for Pomona and a double exponential for Autumnalis) based on the assumption that serovars have the same underlying decay process.

Note that we did not attempt to model the initial period during which antibody levels increase, which is a limitation imposed by the low temporal resolution of our data relative to the duration of the increase period, which is not well known but is likely somewhere between 1 and 4 weeks (Langston & Heuter, 2003; Levett, 2001). When data do allow quantification of the increase period, the increase and decrease phases are typically modelled as two different functions connected at the peak antibody level time (de Graaf et al., 2014; Teunis et al., 2016).

2.3 | Model fitting

Model fitting was done using Bayesian MCMC as implemented in rJAGS (Plummer, 2019). A log-normal error distribution was assumed for antibody levels. Six parallel chains were run for 60,000 iterations (10,000 burn-in), assessing chain convergence visually and with the Gelman-Rubin convergence diagnostic (Brooks & Gelman, 1998).

A major advantage of a Bayesian approach is that it allows the explicit incorporation of additional information about parameters through prior distributions. We used informative priors for the time of infection (i.e. peak antibody level time θ_i) and peak antibody level β_i, as described below. We further aimed to capture the biological variation in model parameters across the population, to derive both individual and population-level estimates. This was possible by making the model hierarchical, where the population-level parameters (hyperparameters) were estimated explicitly, and the individual-level parameters were drawn from these population-level distributions (Gelman & Hill, 2007). Individual-level parameters were modelled using prior distributions $\log(\beta_i) \sim \mathcal{N}(\beta_0, \sigma_{\beta_0})$, $\lambda_i \sim \mathcal{N}(\lambda_0, \sigma_{\lambda_0})$, $\log(r_i) \sim \mathcal{N}(r_0, \sigma_{r_0})$ and $\log(v_i) \sim \mathcal{N}(v_0, \sigma_{v_0})$, where $\beta_0, \sigma_{\beta_0}, \lambda_0, \sigma_{\lambda_0}, r_0$ and σ_{r_0} are the hyperparameters of the model: population-level means and standard deviations (SD) of peak antibody level (mean β_0, SD σ_{β_0}), exponential decay rate (mean λ_0, SD σ_{λ_0}) and power function shape (mean r_0, SD σ_{r_0}) and scale (mean v_0, SD σ_{v_0}). Each of these hyperparameters had its own prior distribution (Table S1). Note that when parameters need to be constrained (e.g. $\beta_0 \geq 1$), this must either be modelled using an appropriate prior distribution, or iterations with impossible samples must be removed from the posterior distributions.

Parameter estimation and model performance can be improved by combining data from multiple biomarkers or other covariates such as age, incidence seasonality or other infection risk factors (Borremans et al., 2016). As an example, we implemented an additional biomarker: antibody levels against serovar Autumnalis. This was possible using a joint-likelihood approach (Isaac et al., 2020). This is a simple extension of single-biomarker fitting, where two separate models (for Pomona and Autumnalis) are fitted simultaneously, with distinct values allowed for all parameters except the peak antibody time θ_i, which becomes a shared parameter. This approach increases the likelihood of accepting parameter values that are supported by the different biomarker datasets and can result in more precise posterior estimates for θ_i. Last, to account for the correlated Pomona and Autumnalis antibody levels a multivariate normal distribution for both peak antibody parameters was used.

Because samples were processed at two different labs an additive lab effect parameter was added to the model. This allows for antibody levels of the labs to differ systematically.

The JAGS code used for model fitting has been provided as Supporting Information and in the Rmarkdown code. Posterior 95% credible intervals (CrI) were calculated as highest density intervals using the function 'dens' of R package HDINTERVAL (Meredith & Kruschke, 2018).

2.4 | Prior distribution of peak antibody time

Peak antibody time θ_i was bounded by the interval between the most recent negative sample (negative test or birth date) and the first positive sample (the infection window). This information was incorporated as a uniform prior distribution for θ_i with minimum

θ_{min} and maximum 0. Alternative data to inform θ_i could be average lifespan, known seasonality in infection risk, onset of clinical signs of disease, or any other variable that provides information about the possible infection time. The probability distribution translating this information to a prior distribution can assume any shape and is not restricted to a uniform distribution as used here for the bounded infection window. We emphasize again that peak antibody time θ_i is used as a proxy for time of infection, since the time resolution of the dataset makes it highly unlikely that sufficient samples were taken in the period between infection and peak antibody time.

2.5 | Prior distribution of peak antibody level

Another source of information that was used to improve model fitting is the distribution of peak antibody levels of recently infected foxes, which informs the population-level mean β_0 and standard deviation σ_{β_0}. This prior distribution was chosen by selecting a subset of foxes with relatively short infection windows, balancing the trade-off between sample size, which must be sufficiently large to provide a useful distribution, and recent infection time. We chose a maximum time of 250 days between the first positive and last negative sample as "recently infected". Although this was still a large window, this was a limitation resulting from the study's sampling frequency, which provides an opportunity to illustrate the strength of the approach under realistic field conditions. This resulted in 54 foxes that could be used to inform the prior distribution. Normal distributions were fitted to the frequency distribution of the antibody levels of the first positive samples. Fitted means were increased slightly to account for antibody decay within the 250-day window, as were standard deviations to allow for additional uncertainty, resulting in prior distributions with mean 7 and sd 2.5 $\log_2$ dilutions for serovar Pomona and mean 7.5 and sd 3 $\log_2$ dilutions for serovar Autumnalis. Normal distributions were fitted using the fitdistr function in R package MASS (Venables & Ripley, 2002). More details are provided in Supporting Information (Section 1). Note that the fact that this subset of individuals is used for informing a prior as well as being included in the model technically means that these data are being used twice to estimate peak antibody level. For this reason, the standard deviation of the prior distribution was deliberately chosen to be larger, which minimizes this effect. This is a way to allow this subset of individuals, which is known to provide better information about peak antibody level than the rest of the dataset, to weigh slightly more heavily on the estimation of peak antibody level. As shown in Supporting Information (Section 2), the shape of the prior has a very limited influence on parameter estimates. In addition, we tested whether this approach affected the model estimates by using the same procedure for everything, except the prior distribution of peak antibody level was selected using only the 10 animals that had the shortest time between last negative and first positive, and then those 10 animals were withheld from all model fitting. This resulted in nearly identical parameter estimates (results not included).

2.6 | Data for model fitting

Model fitting was done using 1381 data points from 305 foxes that had at least two positive samples preceded by a negative one (or a known birth date) that determines the infection window. Because the antibody model does not accommodate secondary increases in antibody level, samples that exhibited signs of possible antibody boosting (possibly due to re-exposure to the pathogen, not necessarily leading to infection), defined here as an antibody level increase ≥2 $\log_2$ units between samples, were removed from the dataset together with all samples from that individual that were taken afterwards. This occurred in 2 out of the 305 foxes, resulting in the removal of 4 data points.

2.7 | Model comparison

Model fits were compared using the leave-one-out cross-validation information criterion LOOIC (Vehtari et al., 2017) using R package LOO (Vehtari et al., 2020), where lower values indicate a better fit. Additionally, we used three measures of the degree to which a model improves the estimation of peak antibody time θ_i relative to the uniform prior infection window. The first is "% infection window reduction" which is the percentage by which the size of the infection window was reduced in the posterior distribution compared to the original uniform window size, for credible intervals of 95% (a commonly used interval) and 50% (a better representation of the most concentrated area of the posterior). For example, if the original window size is 250 days, and the model generates a posterior distribution of θ_i for which the 95% CrI ranges from 200 to 20 days prior, the % reduction would be $100 - \left(\frac{200-20}{250*0.95}\right) * 100 = 24\%$. If the 50% CrI of the posterior ranges from 110 to 75 days prior, the % reduction would be $100 - \left(\frac{140-65}{250*0.5}\right) * 100 = 40\%$. While these measures are useful because they are easy to interpret, they do not consider that probabilities within the credible intervals are not equal, and some θ_i will have a higher probability than others. To capture this, we used relative entropy (or Kullback–Leibler divergence; Kullback & Leibler, 1951) as a third measure. Relative entropy (units = "bits") quantifies the difference in information content between two distributions, which in this case are the uniform prior distribution (infection window) and the posterior distribution of θ_i. Relative entropy $D_{KL}(P \mid\mid Q) = \sum_x P(x)\log_2 \frac{P(x)}{Q(x)}$, where $P(x)$ and $Q(x)$ are the posterior and prior distributions defined over the same range of values x (Burnham & Anderson, 2002). The values of x are individual-specific and adopt every possible value of θ_i as determined by the uniform prior infection window. A higher value corresponds with more information in the posterior relative to the uniform prior. For reference, given a uniform prior (original infection window) of 250 days, a posterior normally distributed around a mean of 100 days with a standard deviation of 20 would result in a relative entropy value of 1.6 bits, compared to 0.8 bits if the standard deviation is 35; that is, a higher relative entropy value indicates a greater reduction in uncertainty about estimated infection time.

2.8 | Simulation study

To assess model behaviour to different assumptions and conditions, we simulated data mimicking the real dataset. Antibody levels were simulated for 75 individuals, randomly sampling log peak antibody level and decay rate from normal distributions and drawing two to five samples (up to 2000 days after peak antibody level). Random noise was added to antibody levels to simulate real variation. The peak antibody sample was excluded from the simulated dataset, again to mimic reality. Parameter estimation was done for multiple simulated datasets that were generated using a range of standard deviations for peak antibody level and decay rate. We then tested how different combinations of peak antibody level variation and decay rate affect model performance, as faster decay and/or smaller variation in peak antibody level may constrain the possible peak antibody time window, which in turn would affect the precision of the peak antibody time θ_i estimates. Simulation details and results are provided in Supporting Information (Section 2).

2.9 | Additional supplementary analyses

Some analyses were performed to provide additional information and context and are only shown in Supporting Information Section 5 shows tested correlations between peak antibody level and a number of covariates; Section 6 shows the correlation between serovars Pomona and Autumnalis and Section 7 shows peak antibody level estimates for individuals without a prior negative sample and when using only the first positive sample for each individual.

2.10 | Software

All data preparation, analysis and plotting were done in R (R Core Team, 2019) using packages GGPLOT2 (Wickham, 2016), RJAGS (Plummer, 2019), GGRIDGES (Wilke, 2020), DPLYR (Wickham et al., 2019), PATCHWORK (Pedersen, 2019), LOO (Vehtari et al., 2020), R2OPENBUGS (Sturtz et al., 2005) and HDINTERVAL (Meredith & Kruschke, 2018).

3 | RESULTS

3.1 | Model fits to antibody decay data

Of the three candidate models (single exponential, double exponential, power) the best fits were observed for the two that allow faster initial decay that slows with time since peak antibody level (double exponential and power), for both serovar Pomona and Autumnalis (Figure 2a). The double exponential model had the lowest LOOIC value (single exponential = 5933, double exponential = 4705, power = 5757). All models were fit to the dataset including both serovar Pomona and Autumnalis, resulting in one overall LOOIC value but separate parameter estimates for each serovar. Results are shown for the double exponential model only. The fitted double exponential functions for Pomona and Autumnalis are shown in Figure 2b with the observed data after adjusting time (x-axis) for each individual based on the estimated peak antibody time θ_i. The mode was used as the posterior estimate for θ_i to accommodate the skewed posterior distribution.

3.2 | Posterior estimates of decay model parameters

The population-level posterior means of the peak antibody level distribution parameters for serovar Pomona were 6.89 $\log_2$ units (95% CrI 6.61 to 7.15) for the mean and 2.00 $\log_2$ units (95% CrI 1.79 to 2.24) for the standard deviation. The estimated peak antibody level distribution for serovar Autumnalis was slightly higher, with a mean of 7.45 $\log_2$ units (95% CrI 7.11 to 7.88) and standard deviation of 2.08 $\log_2$ units (95% CrI 1.81 to 2.35; Figure 3a).

The population-level distribution of the decay rate parameter for serovar Pomona had a mean of 0.00086 $\log_2$ units/day (95% CrI 0.00079 to 0.00093) and standard deviation of 0.00035 $\log_2$ units/day (95% CrI 0.00028 to 0.00042). For serovar Autumnalis the mean was 0.00069 $\log_2$ units/day (95% CrI 0.00061 to 0.00078) and the standard deviation was 0.00028 $\log_2$ units/day (95% CrI 0.00021 to 0.00037; Figure 3b). There was no statistically meaningful correlation between individual peak antibody level and decay rate
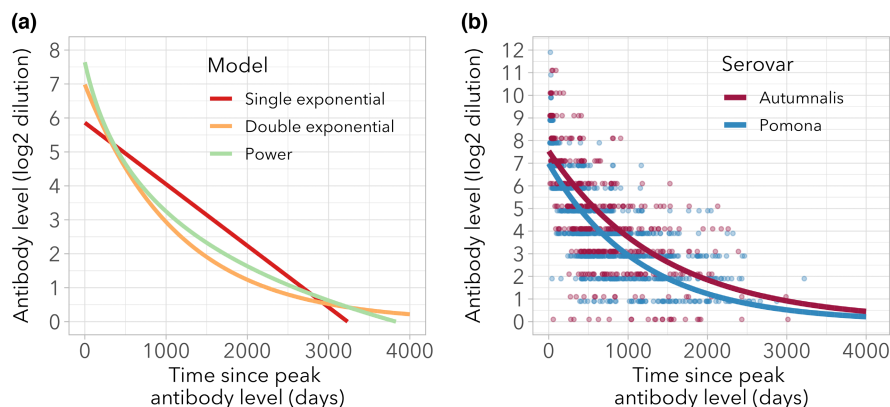
FIGURE 2 Candidate functions fitted to observed data. (a) Fitted functions for the three candidate models, using the posterior means for serovar Pomona peak antibody level and decay rate. (b) Fitted double exponential functions for serovars Pomona and Autumnalis, overlaid on observed data for 307 individuals after changing time since first positive sample to estimated time since peak antibody level.
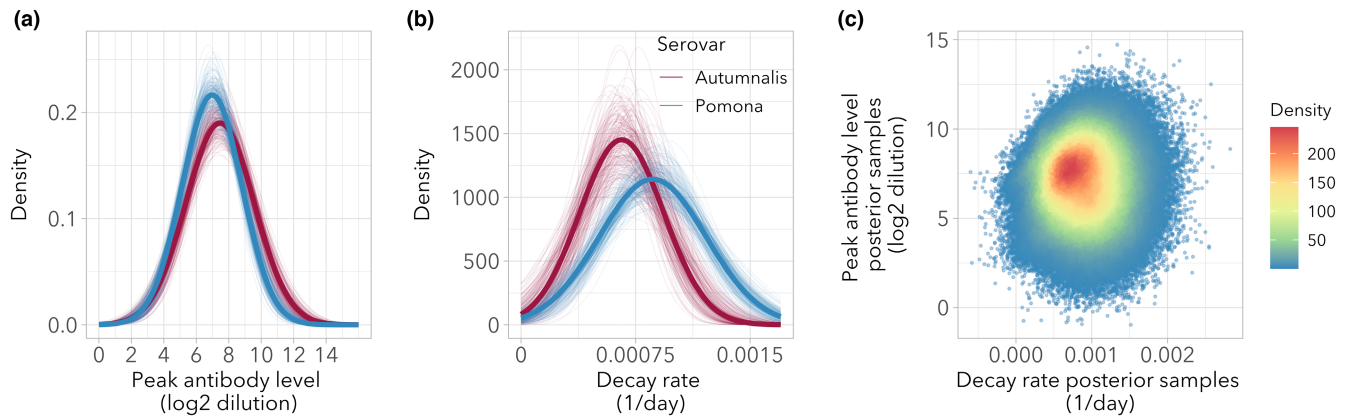
FIGURE 3 Estimated population-level distributions of peak antibody level (a) and decay rate (b), for serovars Pomona and Autumnalis. Bold lines are the distributions based on the posterior means of the mean and the standard deviation of each parameter. Thin lines are drawn from a random selection of 200 MCMC iterations, to show the magnitude of the variation around the posterior mean values. Panel (c) shows posterior samples for peak antibody level and decay rate, with colours depicting the density of points.

(posterior mean of the fitted regression coefficient φ in $\theta_i = \varphi\lambda_i$: 90, 95% CrI −456 to 646; Figure 3c).

The mean percentage by which the individual prior infection windows were reduced after model fitting (using 50% credible intervals of the posterior distribution) was 22.1% (±1.1 SE, range 2.5% to 83.2%) for the model that includes both serovars (with nearly identical results for the model using serovar Pomona only). When using 95% credible intervals, mean window size reduction for the model including both serovars was 6.1% (±0.5 SE, range 0.5% to 64.8%) for the model that includes both serovars (with nearly identical results for the model using serovar Pomona only). Mean relative entropy values were 0.100 bits (±0.011 SE, range 0.006 to 1.185) and 0.107 bits (±0.014 SE, range 0.006 to 1.691).

3.3 | Correlates of model precision

We observed strong individual variation in how much information the model was able to provide about peak antibody time θ_i, with reductions in infection window size ranging from 2.5% to 83.2% (or 0.5% to 64.8% using a 95% credible interval), and relative entropy values from 0.006 to 1.185 bits. To explore the factors underlying this variation, we tested the correlation between window size reduction (using the 95% CrI, which is highly correlated with the 50% CrI) and a number of variables: prior infection window size, number of samples, time range covered by the samples, estimated peak antibody level and estimated decay rate for serovar Pomona. Correlations were tested using linear models with a log-transformed infection window reduction outcome variable. Greater improvements were observed when the prior infection window was larger (effect size (rel. change) = 1.28, 95% CrI 1.17–1.40), when the estimated decay rate was higher (effect size (rel. change) = 1.47, 95% CrI 1.36–1.59) and when the estimated peak antibody level was higher (effect size (rel. change) = 1.13, 95% CrI 1.04–1.24). Model comparison using LOOIC showed the best fit for a regression model including a combination of decay rate, peak antibody level and infection

window size, with decay rate occurring in all top models (Supporting Information Section 3). In short, more information is gained when the early antibody levels are high (leading to high estimates of peak titre, and rapid decay) and when the possible infection window is long (meaning there is more room for improvement). This is illustrated in Figure 4, which shows the detailed output for two different individuals, while Figure 5 shows the posterior distributions of θ_i for each individual.

3.4 | Simulation study

The models fitted to simulated data were able to accurately estimate the population-level parameters (β_0, σ_{β_0}, λ_0 and σ_{λ_0}; Figure S2) across a broad range of assumptions about peak antibody level mean and standard deviation, showing that the modelling approach works well. The estimation of parameter values at the individual level was good overall, but performance declined with more extreme values of the "true" individual peak antibody level (i.e. when the real simulated level was much lower or higher than the population mean; Figures S3–S6).

Of broader relevance to biomarker dynamics in general, we found that model performance was strongly dependent on both decay rate and variation in peak antibody level (σ_{β_0}). Infection window reduction increased strongly with decay rate and correlated negatively with peak antibody level variation (Table 1). Figure S8 illustrates how estimates of peak antibody time θ_i will be more accurate with faster decay and/or smaller variation in peak antibody values in the population.

4 | DISCUSSION

One of the outstanding challenges in quantitative serology is how to estimate the time of infection from antibody levels in the absence of experimental data (Borremans et al., 2016; Pepin et al., 2017). By
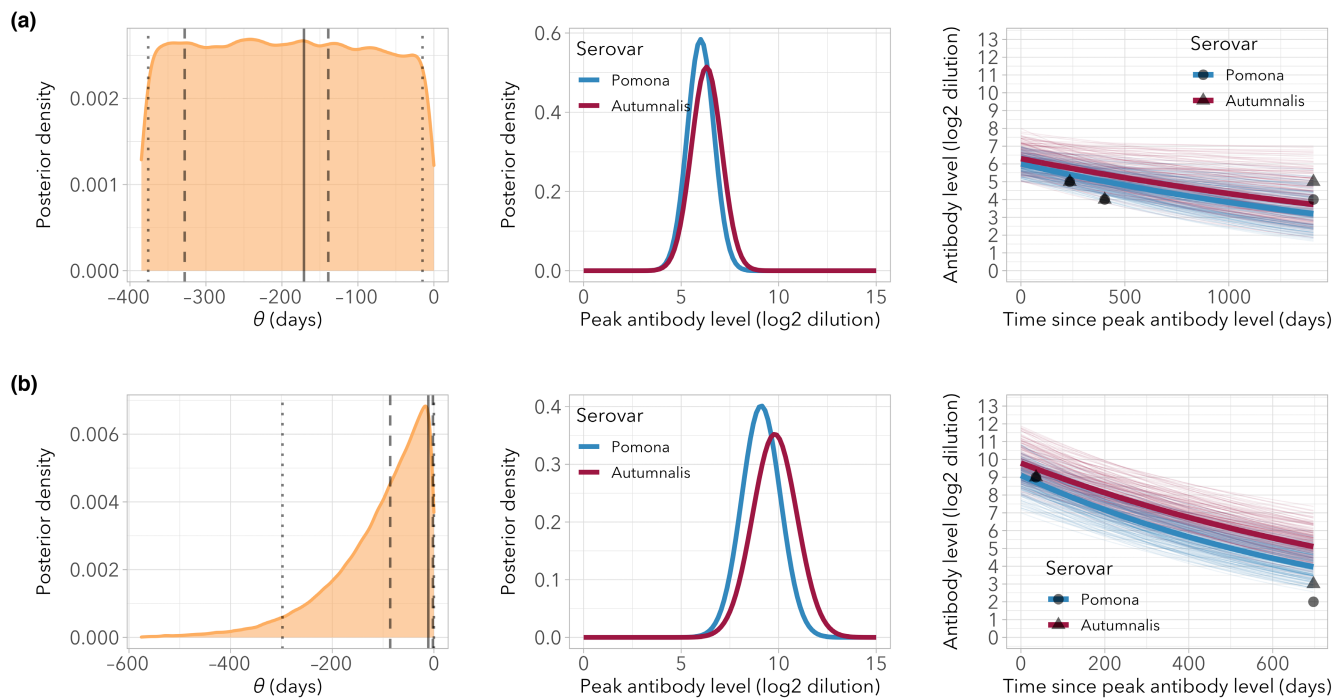
FIGURE 4 Posterior results for two individual foxes with low (a) and high (b) gain in information about peak antibody time *θ*. Left: posterior distribution of *θ*, the time between the first positive sample and the estimated peak antibody time, with maximum density (bold line) and credible intervals (95% = dotted line, 50% = dashed line). Center: posterior density for peak antibody level. Right: fitted functions using posterior estimates (bold lines) overlaid on 200 randomly selected iterations to show the distribution; black points are the observed samples.

integrating data from different sources using a Bayesian approach, we were able to estimate the time of infection and model antibody decay despite highly imprecise knowledge about when individuals were infected. Two key sources of prior information were used in the model. The first is information about possible peak antibody levels provided by a subset of foxes known to have been infected relatively recently. The second is the infection window, an interval that bounds each individual's possible times at which antibody levels must have peaked, defined by a negative sample preceding the first positive one. Additionally, the Bayesian approach enabled leveraging data from multiple biomarkers, in this case, antibody level data on *Leptospira interrogans* serovar Autumnalis in addition to serovar Pomona.

Model fit statistics showed a clear preference for the two models in which antibody decay decelerates with time, and of those the more parsimonious double exponential model received the highest level of support. Using the posterior means for the double exponential model, the decelerating decay when starting at a Pomona antibody dilution 1:6400 would translate to 198 days to decay to 1:3200, 431 days to 1:1600 and 2495 days to 1:100. Initially rapid antibody decay followed by a slow phase seems to be relatively common and has for example been observed for leptospirosis in California sea lions (Prager et al., 2020), *Bordetella pertussis* in humans (Teunis et al., 2016) and arenavirus in multimammate mice (Borremans et al., 2015). This phenomenon may be a consequence of the heterogeneous dynamics of antibodies produced at different

sites and different cell populations in the body, at different rates and driven by different mechanisms (Andraud et al., 2012; Teunis et al., 2016; Traggiai et al., 2003).

There was a strong correlation between antibodies against serovars Pomona and Autumnalis, which was particularly strong for peak antibody levels. This meant that the information gained by the addition of data on serovar Autumnalis was limited, as that information was for the most part already provided by serovar Pomona. We indeed found that the reduction in infection window size achieved using our model was not much better when integrating data on both serovars versus only using serovar Pomona. This is a useful general insight into what to expect when considering incorporating multiple biomarkers for quantitative serology, and suggests that a useful strategy would be to prioritize biomarkers that do not correlate strongly. For instance, combining antibody data with data on the presence of a pathogen (or its genetic material) is likely to be much more informative than data on an antibody exhibiting the same dynamics, as shown for arenavirus infection in the rodent *Mastomys natalensis* (Borremans et al., 2016), hantavirus in *Peromyscus* sp. mice (Abbott et al., 1999) and influenza A in swine (Strelioff et al., 2013). Alternatively, biomarkers that reflect the state of disease (e.g. renal health) can add useful information (Prager et al., 2020).

The degree to which the model was able to improve individual infection windows correlated strongly with a number of individual variables. The model yielded greater reductions in infection window with higher decay rate, higher peak antibody level and greater size
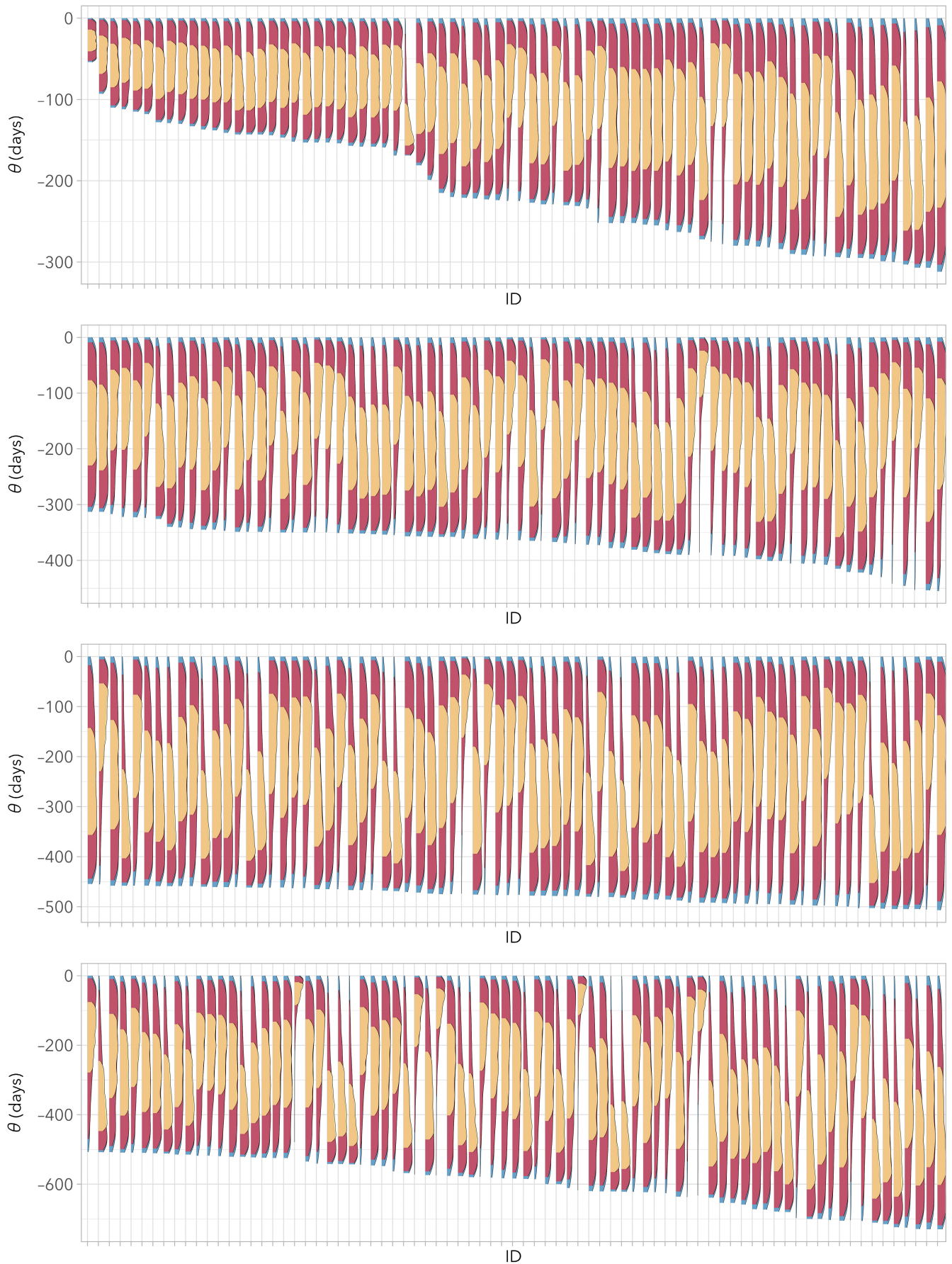
FIGURE 5 Posterior densities of peak antibody time θ for all foxes. Densities were plotted along the *y*-axis to enable showing all individuals, ordered along the *x*-axis by prior infection window size (full posterior density = blue, density within 95% CrI = red, density within 50% CrI = yellow). Note that the *y*-axis ranges increase from the top to bottom plots.

TABLE 1 Effect of variation in peak antibody level and decay rate on infection window estimation. Gained information on peak antibody time relative to the prior knowledge, a uniform interval bound by the last negative and first positive samples. Values show the percentage by which 95% of the infection window size was reduced, where the 95% CrI of the posterior distribution was taken as the new window. Results were similar when using relative entropy (Table S5). Figure S7 illustrates the different decay rates.

Infection window reduction (%)				
Peak Ab SD (log$_2$ units)	Decay rate (log$_2$ units/day)			
	0.005	0.001	0.0005	0.0001
0.5	46	49	36	6
1.0	44	37	23	3
2.0	37	26	12	2
3.0	34	17	9	1

of the prior infection window size. The latter can be explained by the fact that when the prior infection window is longer, larger improvements are possible. Higher decay rates on the other hand mean that the information conveyed by antibody levels will be more localized in time, thus resulting in better estimates of peak antibody time (Table 1 and Figure S8). The effect of a higher level of peak antibody results from the fact that decay is faster at higher levels. Last, both the data and the simulations showed that a broader distribution of possible peak antibody levels directly translates into a broader distribution of possible peak antibody times, which means that lower individual variation will result in better estimates of the time of infection (Table 1). It is important to note that while these correlations exist in theory, they will only provide an advantage in practice if sufficient data are available, at sufficiently short sampling intervals relative to the decay rate, to accurately capture the antibody decay parameters. This means that in situations where a high decay rate is expected, the frequency of sampling should ideally be high enough to capture the rapid change in antibody levels. If this is not the case, the decay rate parameter will be estimated with a larger degree of uncertainty, leading in turn to more uncertain estimates of the infection window. For determining an optimal sampling strategy prior to a study, a simulation study is recommended (Blaizot et al., 2019).

These characteristics related to model performance are intrinsic to a pathogen-host system and will determine the upper level of performance of any model. For our system, the model yielded reductions in infection window size ranging from small (2.5% using 50% credible intervals) to impressive (83%); these reductions were obtained despite the relatively slow decay of antibodies against *L. interrogans* serovar Pomona in island foxes as well as considerable variation in peak antibody level. Indeed, the estimated decay rate of 0.0009 log$_2$ units/day results in a window of 320 days between antibody levels 8 and 6 log$_2$ units (assuming a peak level of 11). For comparison, decay rates of 0.005 and 0.01 log$_2$ units/day would result in windows of 58 and 29 days, respectively. This means that for other systems such as *L. interrogans* serovar Pomona infection in California sea lions *Zalophus californianus* where antibody decay can be as fast

as 0.058 (Prager et al., 2020), a similar model would be expected to yield considerably more precise estimates of peak antibody time.

Correct inference about the antibody model dynamic parameters and estimated time of infection depends on the choice of candidate models of antibody decay. While the fit of different candidate models to the available data can be compared so that the best-fitting model can be selected, ultimately if all candidate models are highly misspecified this can lead to false confidence in infection times. As for any mode, it is therefore important to choose candidate models carefully, based on existing literature, data and expert knowledge. For example, if antibody decay is much faster in the first weeks after infection than in later periods, but none of the candidate models allow for a varying decay rate, the resulting confidence in infection times might be incorrect.

Quantitative serology is a growing field with major potential (Gilbert et al., 2013; Held et al., 2019; Pepin et al., 2017; Teunis et al., 2012; Wilber et al., 2020), but its broad adoption has been relatively limited due to a number of outstanding challenges. Here, we provided a complete approach to constructing biomarker models entirely from field data with sparse sampling points and unknown infection times, using a hierarchical Bayesian framework that can leverage multiple sources of information and multiple data types (Figure 1). This addresses a major challenge in quantitative serology and time-of-infection estimation that has been one of the key barriers to application to wildlife systems. Within the context of the broader field of quantitative serology the approach can facilitate the adoption in wildlife pathogen systems of methods developed for human pathogens. For example, combining our approach with the powerful methods provided in the SERO-SOLVER R package (Hay et al., 2020) could result in a new toolkit for estimating individual infection history and attack rate in wildlife systems where antibody kinetics have been challenging to model. The package further includes models to deal with antibody boosting follow re-exposure, and exposure to multiple strains that can cause antibody cross-reactivity, which can both be important in wildlife systems.

In conclusion, this work opens new frontiers for quantitative analysis of infectious disease dynamics, including incidence reconstruction with proper error propagation, anamnestic immune response following re-exposure (boosting), dealing with antibody cross-reactivity, integration of infection time estimation and transmission modelling, and software development for easy integration of data sources and incidence reconstruction. The hierarchical structure of the model further provides a natural way to extend it to estimate correlates of infection and biomarker dynamics at the population level and the within-host level.

AUTHOR CONTRIBUTIONS

Benny Borremans, Niel Hens, K. C. Prager and James O. Lloyd-Smith contributed to conceptual development. Benny Borremans, Niel Hens, Riley O. Mummah and James Lloyd-Smith contributed to mathematical development. Benny Borremans performed the analyses. Angela Guglielmino collected the data. Renee L. Galloway

analysed the samples. Benny Borremans wrote the first draft. All authors contributed substantially to revisions.

CONFLICT OF INTEREST STATEMENT
The authors declare that no conflicts of interest exist.

PEER REVIEW
The peer review history for this article is available at https://www.webofscience.com/api/gateway/wos/peer-review/10.1111/2041-210X.14165.

DATA AVAILABILITY STATEMENT
The data and code necessary to reproduce the analyses are available at github.com/bennyborremans/antibody_decay_field_data, and the latest release can be found on Zenodo https://doi.org/10.5281/zenodo.7995965 (Borremans et al., 2023).

ORCID
Benny Borremans https://orcid.org/0000-0002-7779-4107
Riley O. Mummah https://orcid.org/0000-0002-4542-3483
Renee L. Galloway https://orcid.org/0000-0003-4627-0906
Niel Hens https://orcid.org/0000-0003-1881-0637
K. C. Prager https://orcid.org/0000-0003-0669-0754
James O. Lloyd-Smith https://orcid.org/0000-0001-7941-502X

REFERENCES
Abbott, K. D., Ksiazek, T. G., & Mills, J. N. (1999). Long-term hantavirus persistence in rodent populations in Central Arizona. *Emerging Infectious Diseases*, 5(1), 102–112 Retrieved from http://www.pubmedcentral.nih.gov/articlerender.fcgi?artid=2627700&tool=pmcentrez&rendertype=abstract

Andraud, M., Lejeune, O., Musoro, J. Z., Ogunjimi, B., Beutels, P., & Hens, N. (2012). Living on three time scales: The dynamics of plasma cell and antibody populations illustrated for hepatitis a virus. *PLoS Computational Biology*, 8(3), e1002418. https://doi.org/10.1371/journal.pcbi.1002418

Antia, A., Ahmed, H., Handel, A., Carlson, N. E., Amanna, I. J., Antia, R., & Slifka, M. (2018). Heterogeneity and longevity of antibody memory to viruses and vaccines. *PLoS Biology*, 16(8), e2006601. https://doi.org/10.1371/journal.pbio.2006601

Begon, M., Telfer, S., Burthe, S., Lambin, X., Smith, M. J., & Paterson, S. (2009). Effects of abundance on infection in natural populations: Field voles and cowpox virus. *Epidemics*, 1(1), 35–46. https://doi.org/10.1016/j.epidem.2008.10.001

Blaizot, S., Herzog, S. A., Abrams, S., Theeten, H., Litzroth, A., & Hens, N. (2019). Sample size calculation for estimating key epidemiological parameters using serological data and mathematical modelling. *BMC Medical Research Methodology*, 19(51), 1–12. https://doi.org/10.1186/s12874-019-0692-1

Bolker, B. M. (2008). *Ecological models and data in R*. https://doi.org/10.1016/j.phrs.2010.10.003

Boni, M., Molbak, K., & Krogfelt, K. (2019). Inferring the time of infection from serological data. In L. Held, N. Hens, P. O'Neill, & J. Wallinga (Eds.), *Handbook of infectious disease data analysis* (pp. 287–303). Chapman & Hall/CRC Press.

Borremans, B., Hens, N., Beutels, P., Leirs, H., & Reijniers, J. (2016). Estimating time of infection using prior serological and individual information can greatly improve incidence estimation of human and wildlife infections. *PLoS Computational Biology*, 12(5), e1004882. https://doi.org/10.1371/journal.pcbi.1004882

Borremans, B., Leirs, H., Gryseels, S., Günther, S., Makundi, R., & de Bellocq, J. G. (2011). Presence of Mopeia virus, an African arenavirus, related to biotope and individual rodent host characteristics: Implications for virus transmission. *Vector-Borne and Zoonotic Diseases*, 11(8), 1125–1131. https://doi.org/10.1089/vbz.2010.0010

Borremans, B., Mummah, R. O., Guglielmino, A. H., Galloway, R. L., Hens, N., Prager, K. C., & Lloyd-Smith, J. O. (2023). *Github repository on Zenodo*. https://doi.org/10.5281/zenodo.7995965

Borremans, B., Vossen, R., Becker-Ziaja, B., Gryseels, S., Hughes, N., Van Gestel, M., Van Houtte, N., Günther, S., & Leirs, H. (2015). Shedding dynamics of Morogoro virus, an African arenavirus closely related to Lassa virus, in its natural reservoir host *Mastomys natalensis*. *Scientific Reports*, 5, 10445. https://doi.org/10.1038/srep10445

Brookmeyer, R., & Gail, M. (1988). A method for obtaining short-term projections and lower bounds on the size of the AIDS epidemic. *Journal of the American Statistical Association*, 83(402) Retrieved from http://amstat.tandfonline.com/doi/abs/10.1080/01621459.1988.10478599, 301–308.

Brooks, S. P., & Gelman, A. (1998). General methods for monitoring convergence of iterative simulations. *Journal of Computational and Graphical Statistics*, 7(4), 434–455. https://doi.org/10.1080/10618600.1998.10474787

Burnham, K. P., & Anderson, D. R. (2002). Model selection and multi-model inference: A practical information-theoretic approach. *Ecological Modelling*, 172, 96–97. https://doi.org/10.1016/j.ecolmodel.2003.11.004

Caley, P., & Hone, J. (2004). Disease transmission between and within species, and the implications for disease control. *Journal of Applied Ecology*, 41(1), 94–104. https://doi.org/10.1111/j.1365-2664.2004.00867.x

Coonan, T. J. (2010). *Decline and recovery of the Island Fox: A case study for population recovery*. https://doi.org/10.1017/CBO9781107415324.004

Coonan, T. J., Guglielmino, A., & Shea, R. (2015). *Island fox recovery program Channel Islands National Park 2014 annual report*. Retrieved from https://irma.nps.gov/DataStore/DownloadFile/528758

Craft, M. E. (2015). Infectious disease transmission and contact networks in wildlife and livestock. *Philosophical Transactions of the Royal Society B: Biological Sciences*, 370, 20140107. https://doi.org/10.1098/rstb.2014.0107

de Graaf, W. F., Kretzschmar, M. E. E., Teunis, P. F. M., & Diekmann, O. (2014). A two-phase within-host model for immune response and its application to serological profiles of pertussis. *Epidemics*, *9*, 1–7. https://doi.org/10.1016/j.epidem.2014.08.002

Epstein, J. H., Baker, M. L., Zambrana-Torrelio, C., Middleton, D., Barr, J. A., DuBovi, E., Dubovi, E., Boyd, V., Pope, B., Todd, S., Crameri, G., Walsh, A., Pelican, K., Fielder, M. D., Davies, A. J., Wang, L.-F., & Daszak, P. (2013). Duration of maternal antibodies against canine distemper virus and hendra virus in Pteropid bats. *PLoS ONE*, *8*(6), 1–8. https://doi.org/10.1371/journal.pone.0067584

Gelman, A., & Hill, J. (2007). *Data analysis using regression and multilevel/hierarchical models*. Cambridge University Press.

Gilbert, A. T., Fooks, A. R., Hayman, D. T. S., Horton, D. L., Müller, T., Plowright, R., Peel, A. J., Bowen, R., Wood, J. L., Mills, J., Cunningham, A. A., & Rupprecht, C. E. (2013). Deciphering serology to understand the ecology of infectious diseases in wildlife. *EcoHealth*, *10*, 298–313. https://doi.org/10.1007/s10393-013-0856-0

Handel, A., & Rohani, P. (2015). Crossing the scale from within-host infection dynamics to between-host transmission fitness: A discussion of current assumptions and knowledge. *Philosophical Transactions of the Royal Society B: Biological Sciences*, *370*(1675), 20140302. https://doi.org/10.1098/rstb.2014.0302

Hardestam, J., Karlsson, M., Falk, K. I., Olsson, G. E., Klingström, J., & Lundkvist, Å. (2008). Puumala hantavirus excretion kinetics in bank voles (*Myodes glareolus*). *Emerging Infectious Diseases*, *14*(8), 1209–1215. https://doi.org/10.3201/eid1408.080221

Hawley, D. M., Grodio, J., Frasca, S., Kirkpatrick, L., & Ley, D. H. (2011). Experimental infection of domestic canaries (*Serinus canaria domestica*) with mycoplasma gallisepticum: A new model system for a wildlife disease. *Avian Pathology*, *40*(3), 321–327. https://doi.org/10.1080/03079457.2011.571660

Hay, J. A., Minter, A., Ainslie, K. E. C., Lessler, J., Yang, B., Cummings, D. A. T., … Riley, S. (2020). An open source tool to infer epidemiological and immunological dynamics from serological data: Serosolver. *PLoS Computational Biology*, *16*(5), 1–24. https://doi.org/10.1371/journal.pcbi.1007840

Heisey, D., Joly, D., & Messier, F. (2006). The fitting of general force-of-infection models to wildlife disease prevalence data. Abstract—UK PubMed Central. *Ecology*, *87*(9), 2356–2365. Retrieved from http://ukpmc.ac.uk/abstract/MED/16995636

Held, L., Hens, N., & O'Neill, P. (2019). In J. Wallinga (Ed.), *Handbook of infectious disease data analysis*. Chapman & Hall/CRC Press.

Hens, N., Aerts, M., Faes, C., Shkedy, Z., Lejeune, O., Van Damme, P., & Beutels, P. (2010). Seventy-five years of estimating the force of infection from current status data. *Epidemiology & Infection*, *138*(6), 802–812.

Isaac, N. J. B., Jarzyna, M. A., Keil, P., Dambly, L. I., Boersch-Supan, P. H., Browning, E., Freeman, S. N., Golding, N., Guillera-Arroita, G., Henrys, P. A., Jarvis, S., Lahoz-Monfort, J., Pagel, J., Pescott, O. L., Schmucki, R., Simmonds, E. G., & O'Hara, R. B. (2020). Data integration for large-scale models of species distributions. *Trends in Ecology & Evolution*, *35*(1), 56–67. https://doi.org/10.1016/j.tree.2019.08.006

Kullback, S., & Leibler, R. (1951). On information and sufficiency. *Annals of Mathematical Statistics*, *22*(1), 79–86. https://doi.org/10.1214/aoms/1177729694

Langston, C. E., & Heuter, K. J. (2003). Leptospirosis. A re-emerging zoonotic disease. *The Veterinary Clinics Small Animal Practice*, *33*(4), 791–807. https://doi.org/10.1016/S0195-5616(03)00026-3

Levett, P. N. (2001). Leptospirosis. *Clinical Microbiology*, *14*(2), 296–326. https://doi.org/10.1128/CMR.14.2.296

Levett, P. N. (2003). Usefulness of serologic analysis as a predictor of the infecting serovar in patients with severe leptospirosis. *Clinical Infectious Diseases*, *36*(4), 447–452. https://doi.org/10.1086/346208

Meredith, M., & Kruschke, J. (2018). *HDInterval: Highest (posterior) density intervals*.

Mummah, R. O. (2021). *Leptospira in the coastal California ecosystem: Challenges and solutions for analyzing complex wildlife disease data*. University of California.

Pedersen, T. L. (2019). *patchwork: The composer of plots*.

Pepin, K. M., Kay, S. L. S., Golas, B., Shriner, S., Gilbert, A., Miller, R. S., Graham, A. L., Riley, S., Cross, P. C., Samuel, M. D., Hooten, M. B., Hoeting, J. A., Lloyd-Smith, J. O., Webb, C. T., & Buhnerkempe, M. (2017). Inferring infection hazard in wildlife populations by linking data across individual and population scales. *Ecology Letters*, *20*(3), 275–292. https://doi.org/10.1111/ele.12732

Pepin, K. M., Pedersen, K., Wan, X. F., Cunningham, F. L., Webb, C. T., & Wilber, M. Q. (2019). Individual-level antibody dynamics reveal potential drivers of influenza a seasonality in wild pig populations. *Integrative and Comparative Biology*, *59*(5), 1231–1242. https://doi.org/10.1093/icb/icz118

Plummer, M. (2019). *rjags: Bayesian graphical models using MCMC*.

Pothin, E., Ferguson, N. M., Drakeley, C. J., & Ghani, A. C. (2016). Estimating malaria transmission intensity from *Plasmodium falciparum* serological data using antibody density models. *Malaria Journal*, *15*(1), 79. https://doi.org/10.1186/s12936-016-1121-0

Prager, K. C., Buhnerkempe, M. G., Greig, D. J., Orr, A. J., Jensen, E. D., Gomez, F., Galloway, R. L., Wu, Q., Gulland, F. M. D., & Lloyd-Smith, J. O. (2020). Linking longitudinal and cross-sectional biomarker data to understand host-pathogen dynamics: Leptospira in California Sea lions (*Zalophus californianus*) as a case study. *PLoS Neglected Tropical Diseases*, *14*, e0008407. https://doi.org/10.1371/journal.pntd.0008407

R Core Team. (2019). *R: A language and environment for statistical computing*. Retrieved from http://www.r-project.org

Röltgen, K., Powell, A. E., Wirz, O. F., Stevens, B. A., Hogan, C. A., Najeeb, J., Hunter, M., Wang, H., Sahoo, M. K., Huang, C., Yamamoto, F., Manohar, M., Manalac, J., Otrelo-Cardoso, A. R., Pham, T. D., Rustagi, A., Rogers, A. J., Shah, N. H., Blish, C. A., … Boyd, S. D. (2021). Defining the features and duration of antibody responses to SARS-CoV-2 infection associated with disease severity and outcome. *Science Immunology*, *5*(54), 1–20. https://doi.org/10.1126/SCIIMMUNOL.ABE0240

Simonsen, J., Mølbak, K., Falkenhorst, G., Krogfelt, K., Linneberg, A., & Teunis, P. (2009). Estimation of incidences of infectious diseases based on antibody measurements. *Statistics in Medicine*, *28*, 1882–1895. https://doi.org/10.1002/sim.3592

Smith, C., Skelly, C., Kung, N., Roberts, B., & Field, H. (2014). Flying-fox species density—A spatial risk factor for Hendra virus infection in horses in eastern Australia. *PLoS ONE*, *9*(6), e99965. https://doi.org/10.1371/journal.pone.0099965

Strelioff, C. C., Vijaykrishna, D., Riley, S., Guan, Y., Peiris, J. S., & Lloyd-Smith, J. O. (2013). Inferring patterns of influenza transmission in swine from multiple streams of surveillance data. *Proceedings of the Biological Sciences*, *280*(1762), 20130872. https://doi.org/10.1098/rspb.2013.0872

Sturtz, S., Ligges, U., & Gelman, A. (2005). R2WinBUGS: A package for running WinBUGS from R. *Journal of Statistical Software*, *12*(3), 1–16.

Tersago, K., Crespin, L., Verhagen, R., & Leirs, H. (2012). Impact of Puumala virus infection on maturation and survival in bank voles: A capture-mark-recapture analysis. *Journal of Wildlife Diseases*, *48*(1), 148–156. https://doi.org/10.7589/0090-3558-48.1.148

Teunis, P. F. M., van der Heijden, O. G., de Melker, H. E., Schellekens, J. F. P., Versteegh, F. G. A., & Kretzschmar, M. E. E. (2002). Kinetics of the IgG antibody response to pertussis toxin after infection with *B. pertussis*. *Epidemiology and Infection*, *129*(3), 479–489 Retrieved from http://www.pubmedcentral.nih.gov/articlerender.fcgi?artid=2869909&tool=pmcentrez&rendertype=abstract

Teunis, P. F. M., van Eijkeren, J. C. H., Ang, C. W., van Duynhoven, Y. T. H. P., Simonsen, J. B., Strid, M. A., & van Pelt, W. (2012).

Biomarker dynamics: Estimating infection rates from serological data. *Statistics in Medicine*, *31*(20), 2240–2248. https://doi.org/10.1002/sim.5322

Teunis, P. F. M., van Eijkeren, J. C. H., de Graaf, W. F., Marinović, A. B., & Kretzschmar, M. E. E. (2016). Linking the seroresponse to infection to within-host heterogeneity in antibody production. *Epidemics*, *16*, 33–39. https://doi.org/10.1016/j.epidem.2016.04.001

Traggiai, E., Puzone, R., & Lanzavecchia, A. (2003). Antigen dependent and independent mechanisms that sustain serum antibody levels. *Vaccine*, *21*(S2), 35–37. https://doi.org/10.1016/S0264-410X(03)00198-1

van den Bergh, C., Venter, E. H., Swanepoel, R., & Thompson, P. N. (2019). High seroconversion rate to rift valley fever virus in cattle and goats in far northern Kwazulu-Natal, South Africa, in the absence of reported outbreaks. *PLoS Neglected Tropical Diseases*, *13*(5), e0007296. https://doi.org/10.1371/journal.pntd.0007296

Vaughn, D. W., Green, S., Kalayanarooj, S., Innis, B. L., Nimmannitya, S., Suntayakorn, S., … Nisalak, A. (2000). Dengue viremia titer, antibody response pattern, and virus serotype correlate with disease severity. *Journal of Infectious Diseases*, *181*(1), 2–9. https://doi.org/10.1086/315215

Vehtari, A., Gabry, J., Magnusson, M., Yao, Y., Bürkner, P., Paananen, T., & Gelman, A. (2020). Loo: Efficient leave-one-out cross-validation and WAIC for Bayesian models.

Vehtari, A., Gelman, A., & Gabry, J. (2017). Practical Bayesian model evaluation using leave-one-out cross-validation and WAIC. *Statistics and Computing*, *27*(5), 1413–1432. https://doi.org/10.1007/s11222-016-9696-4

Venables, W. N., & Ripley, B. D. (2002). *Modern applied statistics with S*. https://doi.org/10.1198/tech.2003.s33

Weitz, J. S., Beckett, S. J., Coenen, A. R., Demory, D., Dominguez-Mirazo, M., Dushoff, J., … Zhao, C. Y. (2020). Modeling shield immunity to reduce COVID-19 epidemic spread. *Nature Medicine*, *26*, 849–854. https://doi.org/10.1038/s41591-020-0895-3

Wickham, H., François, R., Henry, L., & Müller, K. (2019). *dplyr*: *A grammar of data manipulation*.

Wickham, H. (2016). *ggplot2*: *Elegant graphics for data analysis*. Springer-Verlag.

Wilber, M. Q., Webb, C. T., Cunningham, F. L., Pedersen, K., Wan, X. F., & Pepin, K. M. (2020). Inferring seasonal infection risk at population and regional scales from serology samples. *Ecology*, *101*(1), 1–9. https://doi.org/10.1002/ecy.2882

Wilke, C. O. (2020). *ggridges*: *Ridgelines plots* in "ggplot2". Retrieved from https://cran.r-project.org/package=ggridges

SUPPORTING INFORMATION

Additional supporting information can be found online in the Supporting Information section at the end of this article.

Figure S1. Antibody levels for a subset of individual foxes that tested negative within at most 250 days (left: serovar Pomona, right: serovar Autumnalis). Fitted distributions are shown in teal, and distributions used as priors are shown in orange.

Figure S2. Posterior estimates of peak antibody level for different prior distributions. True = generated distributions with means 7 (SD 1) and 7.8 (SD 1) for serovars Pomona and Autumnalis, respectively.

Figure S3. Effect of prior peak antibody level means. Posterior densities of peak antibody time, peak antibody level and decay rate for the first half of the 75 simulated individuals. Dots indicate the "real" distributions are posterior densities flipped vertically.

Figure S4. Effect of prior peak antibody level means. Posterior densities of peak antibody time, peak antibody level and decay rate for the second half of the 75 simulated individuals. Dots indicate the "real" simulated value, distributions are posterior densities flipped vertically.

Figure S5. Effect of prior peak antibody level standard deviations. Posterior densities of peak antibody time, peak antibody level and decay rate for the first half of the 75 simulated individuals. Dots indicate the "real" simulated value, distributions are posterior densities flipped vertically.

Figure S6. Effect of prior peak antibody level standard deviations. Posterior densities of peak antibody time peak antibody level and decay rate for the second half of the 75 simulated individuals. Dots indicate the "real" simulated value, distributions are posterior densities flipped vertically.

Figure S7. Antibody decay curves for different decay rates.

Figure S8. The number of days (window size) it takes for antibodies to decay from 8 to 6 $\log_2$ dilution units, for a range of biologically realistic decay rates. The yellow dot marks a decay rate close to the one estimated for serovar Pomona. Inset figures show the decay function for selected decay rates, with the window between antibody levels 8 and 6 indicated with dotted lines.

Figure S9. Infection window reduction (heatmap colors) for key correlates decay rate, infection window size and level of the first positive sample.

Figure S10. Correlation between peak antibody levels for serovars Pomona and Autumnalis. (A): Posterior means of each individual. (B) Posterior MCMC samples of the overall means of peak antibody level for the last 20,000 iterations.

Figure S11. Infection window posterior densities for individuals without a negative sample preceding the first positive sample. Colors indicate the size of the credible intervals (blue = 95%, yellow = 50%). Arbitrarily chosen infection windows up to 2190 days (6 years) were possible.

Figure S12. Infection window posterior densities for individuals with only a single positive sample. Colors indicate the size of the credible intervals (blue = 95%, yellow = 50%). Arbitrarily chosen infection windows up to 2190 days (6 years) were possible. Only individuals with a preceding negative sample are shown (others are included in Figure S11). Densities are sorted by posterior median.

Figure S13. Infection window size reduction using only the first positive sample for each individual. Reduction in infection window size plotted against Pomona antibody level (log2 dilution), with colors indicating the size of the original infection window size (i.e., time between the first positive sample and the last preceding negative).

Table S1. Hyperpriors for the different parameters.

Table S2. Statistics for the correlations between outcome variable '% infection window reduction' and candidate variables, using a 95% credible interval for the infection window posterior. Effect sizes are exponentiated to get relative change and are shown with

95% credible intervals. LOOIC values are shown with standard errors.

Table S3. LOOIC values for linear regression models including single and multiple variables fitted to outcome variable '% infection window reduction'. Sorted by LOOIC value, which are shown with standard errors.

Table S5. Effect of peak antibody level and decay rate on infection window estimation.